Time-resolved dual RNA-Seq reveals extensive rewiring of lung epithelial and pneumococcal transcriptomes during early infection

Rieza Aprianto[1], Jelle Slager[1], Siger Holsappel[1] and Jan-Willem Veening[1,*]

[1]Molecular Genetics Group, Groningen Biomolecular Sciences and Biotechnology Institute, Centre for Synthetic Biology, University of Groningen, Nijenborgh 7, 9747 AG Groningen, The Netherlands.

*Correspondence to: j.w.veening@rug.nl, Tel: +31 (0)50 3632408, @jwveening

Keywords: *Streptococcus pneumoniae*, transcriptomics, dual RNA-Seq, host-pathogen interaction, adherence, lung epithelial cells

Abstract

Streptococcus pneumoniae (pneumococcus) is the main etiological agent of pneumonia. Pneumococcal pneumonia is initiated by bacterial adherence to lung epithelial cells. Infection to the epithelium is a disruptive interspecies interaction involving numerous transcription-mediated processes. Revealing transcriptional changes may provide valuable insights into pneumococcal disease. Dual RNA-Seq allows simultaneous monitoring of the transcriptomes of both host and pathogen. Here, we developed a time-resolved infection model of human lung alveolar epithelial cells by *S. pneumoniae* and assessed transcriptome changes by dual RNA-Seq. Our data provide new insights into host-microbe interactions and show that the epithelial glutathione-detoxification pathway is activated by bacterial presence. We observed that adherent pneumococci, not free-floating bacteria, access host-associated carbohydrates and repress innate immune responses. In conclusion, we provide a dynamic dual-transcriptomics overview of early pneumococcal infection with easy online access (http://dualrnaseq.molgenrug.nl). Further database exploration may expand our understanding of epithelial-pneumococcal interaction, leading to novel antimicrobial strategies.

Graphical Abstract

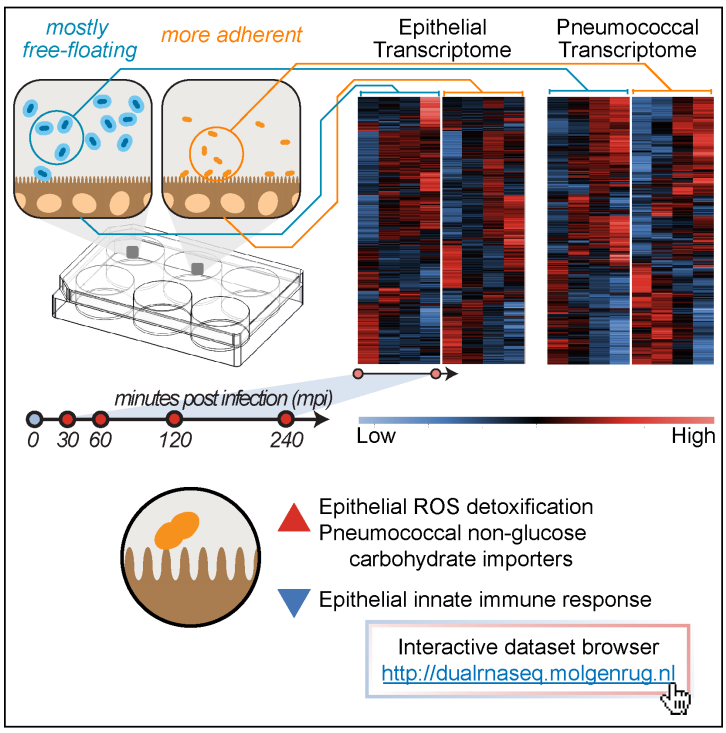

33 ## Introduction

34 Lower respiratory tract infections (LRTIs), or pneumonia, claim more lives than any other
35 communicable disease worldwide; the main etiologic agent behind this infection is the
36 Gram-positive opportunistic pathogen *Streptococcus pneumoniae* (pneumococcus, Prina et
37 al., 2015). Normally part of the human nasopharyngeal microflora, *S. pneumoniae* can
38 invade the lower airways where it provokes host inflammatory and immune
39 responses(Kadioglu et al., 2008). At the earliest stage of infection, pneumococcus adheres
40 to epithelial cells and interacts intimately with the epithelium (Hammerschmidt et al., 2007).
41 Meanwhile, host and pathogen cross-communicate and, they simultaneously, affect each
42 other in a disruptive manner (Kadioglu et al., 2008; Lee et al., 2004). This interspecies
43 interaction activates numerous processes in epithelial and pneumococcal cells (Bootsma et
44 al., 2007; Mlacha et al., 2013). To obtain comprehensive and meaningful biological
45 knowledge of the infection processes involved in pathogenesis, simultaneous monitoring of
46 the transcriptome changes in both species is required (Westermann et al., 2012).

47 Lung epithelial cells perform vital roles during infection. First, the cells form a
48 physical barrier to the external environment. On top of these cells, a thick layer of epithelial-
49 derived mucus offers extra protection that traps and removes pathogens (Voynow and
50 Rubin, 2009). Mucins, the main component of mucus, are large glycoprotein-polymers rich
51 in sialic acids and other aminosaccharides (Rose and Voynow, 2006). Additionally,
52 epithelial cells kill pathogens directly by producing antimicrobial peptides, e.g.: defensins
53 and cathelicidins (Tecle et al., 2010). Moreover, epithelial cells regulate innate immune
54 responses by secreting a wide array of pro-inflammatory cytokines, that recruit neutrophils
55 and activate macrophages (Hallstrand et al., 2014). Finally, epithelial cells activate adaptive

immune cells, including dendritic cells and T-cells via chemokine expression (Soumelis et al., 2002).

Pneumococcal adherence to epithelial cells is the first necessary step to pathogenesis (Bogaert et al., 2004). In order to adhere, pneumococcus must quickly shed the thick exopolysaccharide capsule, which protects against phagocytes (Abeyta et al., 2003; Hyams et al., 2010). The shedding exposes surface adhesion factors and desensitizes the bacterium from antimicrobial peptides (Beiter et al., 2008; Kietzman et al., 2016). Subsequently, *S. pneumoniae* must acquire nutrients to support growth and, at the same time, evade host immune responses (Shelburne et al., 2008). Pneumococcal factors may be involved in multiple processes, e.g.: PsaA, a surface-exposed protein, acts concurrently as adhesion factor and manganese transporter (Rajam et al., 2008). The scarce manganese (Gray et al., 2010) helps in neutralizing reactive oxygen species (ROS) and bacterial fitness (Tseng et al., 2002).

Interspecies interaction during infection is a chaotic process which necessitates rapid and massive adaptation for epithelial and pneumococcal survival. During the adaptation, transcriptional changes plays a focal point both in host(Jenner and Young, 2005) and in pathogen (Sorek and Cossart, 2010). RNA-sequencing (RNA-Seq) delivers genome-wide quantitative snapshots of the transcriptome (Kukurba and Montgomery, 2015). In a thought experiment, Vogel and co-workers argued that simultaneous profiling of host and pathogen transcriptomics by dual RNA-Seq might provide valuable insights for infection biology (Westermann et al., 2012). Recent dual RNA-Seq studies were successful in elucidating the role of sRNAs in the intracellular pathogen *Salmonella typhimurium* (Westermann et al., 2016), cross-talk in the Gram-negative LRTI pathogen *Haemophilus influenzae* (Baddal et

79 al., 2015) and transcription profiles in the protozoan *Leishmania major* (Dillon et al., 2015)
80 during their respective infection.

81 Here, we exploited the dual RNA-Seq approach to simultaneously monitor the
82 transcriptome cross-talk between lung alveolar epithelial cells and pneumococci during
83 early infection. Due to the transient and highly-dynamic nature of the transcriptome
84 (Pedersen et al., 2011), we monitored the transcriptional changes in a time-resolved
85 manner. Moreover, since pneumococcal adherence to epithelial cells determines the
86 outcome of early infection, we compared adherent and non-adherent *S. pneumoniae* to
87 allow specific transcriptional interrogation on adherence. Additionally, we confirmed our
88 dual RNA-Seq gene expression data by qRT-PCR and quantitative fluorescence
89 microscopy to visualize pneumococcal proteins and thereby confirm several novel biological
90 observations identified in the dataset. Finally, we developed a user-friendly online database
91 (http://dualrnaseq.molgenrug.nl), giving access of our detailed time-resolved dual
92 transcriptomes data to the pneumococcal, microbiology, immunology and pulmonology
93 research communities.

94

95 ## Results

96 ### The early pneumococcal infection model to epithelial cells

97 At the first phase of LRTI, *S. pneumoniae* adheres to the sterile apical-side of epithelial
98 cells, adaptation of bacterial transcriptome occurs followed by bacterial outgrowth (Mlacha
99 et al., 2013), which in turn stimulate epithelial transcriptional responses to their presence
100 (Bootsma et al., 2007). We aimed to recapitulate these events in an *in vitro* model
101 consisting of co-incubation of the pathogenic *S. pneumoniae* strain D39 (serotype 2) to a

102 confluent layer of type II lung alveolar human epithelial cell (A549) at a multiplicity of
103 infection (MOI) of 10, i.e., ten pneumococci per epithelial cell (**Figure 1A**). Five time points
104 up to 4 hours after infection were selected to capture both early transcriptome responses
105 (30 and 60 mpi) and later responses (120 and 240 mpi). Six technical replicates (individual
106 wells) were pooled into one biological replicate. Two biological replicates were used for
107 each time point, except for 240 mpi where we only obtained one replicate (**Figure 1E**). In
108 order to elucidate adherence-specific expression, we incorporated an isogenic
109 unencapsulated D39 strain (Δ*cps2E*) with increased adherence to epithelial cells into the
110 model(Kjos et al., 2015). The capsular mutant showed significantly greater capacity to
111 adhere to epithelial cells than its encapsulated parental strain ($p<0.001$, **Figure 1C**). During
112 infection, the total number of cells of both strains were significantly ($p<0.01$) increased after
113 4 hours (**Figure 1D**), showing that both strains multiply in the model, thereby recapitulating
114 one of the characteristics of infection. To minimize transcriptional changes because of
115 sample handling, we did not separate cellular mixtures before total RNA isolation (epithelial
116 cells, adherent pneumococci and free-floating pneumococci, **Figure 1E**, see **Supplemental**
117 **Information**).

118 To analyze the time-resolved dual RNA-Seq dataset, a combination of freely
119 available bioinformatics tools was used (**Figure 1F**). First, raw reads were trimmed (Bolger
120 et al., 2014) and aligned (Dobin et al., 2013) to a chimeric genome containing the
121 concatenated genome of *Homo sapiens* (GRCh38, Ensembl) and *S. pneumoniae* D39
122 (NC_008533.1, NCBI). The one-step mapping was chosen to minimize rates of false
123 negatives. Reads were then separately counted (Liao et al., 2014) and classified as either
124 epithelial or pneumococcal. Following differential gene expression analysis, three groups of
125 genes were removed (see below) and unbiased automatic clustering (Kumar and E.

126 Futschik, 2007) and functional enrichment were performed (Dennis et al., 2003; van
127 Opijnen and Camilli, 2012).

128
129 **Dual RNA-Seq generates high-quality datasets with clusters of epithelial and**
130 **pneumococcal co-expressed genes**

131 Dual RNA-seq generated single end 75 nt reads. We sequenced to such depth, that on
132 average each library has 70 million reads (30 to 95 million). After adapter trimming and
133 removal of low-quality reads, we retained 92% (89.0-93.0%). Subsequently, 79% of reads
134 (74.6 to 83.0%) successfully aligned to the chimeric genome. Additionally, we concluded
135 that dual rRNA depletion was successful since only 0.03% of human and 0.24% of
136 pneumococcal reads mapped as ribosomal RNAs. For each library, we counted 18 million
137 epithelial reads (26%) and 37 million pneumococcal reads (52%, **Figure 2A**). The high
138 number of reads in each library and the high fraction of usable reads highlights the quality
139 and suitability of our approach for dual RNA-Seq: simultaneous total RNA isolation, dual
140 rRNA depletion and cDNA library preparation. PCA analysis showed no evidence for batch
141 effects (**Supplemental Figure 1**). Relative enrichment of pneumococcal reads may stem
142 from the total RNA isolation protocol. Nevertheless, each library contained sufficient
143 epithelial reads for differential gene expression analysis (The ENCODE Consortium, 2011).

144 To simplify further analyses, we excluded three gene fractions (**Figure 2B**). First, we
145 removed unexpressed genes, i.e., without any counts in all libraries: 22.991 (38%) epithelial
146 genes and 24 (1%) pneumococcal genes. The relatively large fraction of unexpressed
147 epithelial genes is in accordance with recent studies on the human epithelial transcriptome
148 (Hackett et al., 2012; St-Pierre et al., 2013). Second, we excluded genes that were
149 differentially expressed ($p<0.05$) at 0 mpi between unencapsulated (Δ*cps2E*) and

150 encapsulated (wt) libraries. While only five epithelial genes were removed, 394 (19%)
151 pneumococcal genes were already differentially expressed at 0 mpi. Although polar effect
152 due to *cps2E* disruption can explain differential expression of genes in the 17kb long *cps*
153 operon, it remains unknown why other genes were differentially expressed. We speculate
154 that constructing the thick exopolysaccharide capsule requires specific transcriptional fine-
155 tuning of numerous genes outside the *cps* locus. Finally, we removed genes with no
156 significant difference (p>0.05) and genes with fold changes less than 2 in all contrasts
157 (**Supplemental Figure 2**). In total, the epithelial working libraries contained 4.009 (7% of
158 total) genes and pneumococcal working libraries 868 (42% of total) genes.

159 To compare gene expression, we normalized expression values using DESeq2
160 (Love et al., 2014), centered and clustered the values (Kumar and E. Futschik, 2007). The
161 centered normalized values were visualized as heat maps, divided into two panels, one for
162 each bacterial strain. Strikingly, heat maps showed obvious clusters of co-expressed genes
163 and clear gene expression differences between adhering (Δ*cps2E*) and non-adhering (wt)
164 bacteria to epithelial cells (**Figure 2CD**). Specifically, the left panel of **Figure 2C** shows the
165 epithelial transcriptional response exposed to encapsulated *S. pneumoniae* at different time
166 points (30, 60, 120 and 240 mpi) while the right panel displays the response in contact with
167 the unencapsulated strain. *Vice versa*, co-expressed clusters in pneumococcal genes are
168 differentially expressed in contact with human epithelial cells (**Figure 2D**).

169 Making raw data publicly-available has been common practice in recent years, as we
170 have done for this project (GEO accession number GSE79595). Unfortunately, publicly
171 available datasets do not translate to direct exploration and extraction of biological insights
172 for the majority of researchers. Therefore, we built an easily-accessible online platform
173 which hosts the complete dual RNA-Seq database. To access and visualize the data, users

174 can simply select the gene of interest (or multiple genes of interests) and examine their
175 expression during early infection (**Supplemental Figure 3**). Expression data can be
176 downloaded and opened in common spreadsheet software e.g.: Microsoft Excel®. To
177 visualize expression, users can choose from three normalization methods: DESeq2
178 normalization(Love et al., 2014), TPM (transcript per million (Wagner et al., 2012) and $\log_2$ -
179 transformed TPM values.

180

181 **Validation of dual RNA-Seq by qRT-PCR and pneumococcal protein fusions**

182 To confirm dual RNA-Seq data by quantitative real-time PCR (qRT-PCR), we chose 10
183 epithelial genes (*ABCC2, AKR1B10, AKR1C3, ALDH1A1, DEFB1, DKK1, IDH1, NOLC1,*
184 *PTGES* and *TXNRD1*) and 19 pneumococcal genes (*amiC, blpY, dinF, hrcA, infC, lytA,*
185 *malC, manL, msmR, nrdD, pulA,* SPD_0249, SPD_0392, SPD_0475, SPD_0961,
186 SPD_0990, SPD_1517, SPD_1711 and SPD_1798). The target genes were selected
187 because of their varied expression profiles: increasing, decreasing or unchanged. The cycle
188 threshold (Ct) for epithelial transcripts were normalized against *ACTB* (β-actin) while
189 pneumococcal transcripts were normalized to *gyrA* (gyrase A). The reference genes were
190 highly expressed and did not show significant changes ($p>0.05$, $FC<2$) between any time
191 points during early infection. The qRT-PCR fold change was calculated by the ΔΔCt method
192 (Livak and Schmittgen, 2001) to one time point. Fold changes obtained by qRT-pCR and
193 dual RNA-Seq showed a relatively high correlation for both species: epithelial transcripts,
194 (R^2=0.72) and pneumococcal transcripts, (R^2=0.73, **Figure 3A**), validating the reliability of
195 dual RNA-Seq data.

196 Since transcript levels do not necessarily correspond with protein expression (Ning
197 et al., 2012; Taniguchi et al., 2010), we quantified four pneumococcal protein levels whose

198 genes showed upregulation during adherence to epithelial cells. We fused a fast-folding
199 variant of the green fluorescent protein (GFP) to the carboxy-termini of SPD_0475,
200 SPD_0963, SPD_1711 and SPD_1716, at their own locus while preserving all upstream
201 regulatory elements (**Figure 3B**). We transformed these constructs into the *hlpA_hlpA-rfp,*
202 Δ*cps2E* genetic background (Kjos et al., 2015). SPD_0475 encodes a 204 amino acids (aa)
203 CAAX amino terminal protease with unknown function. SPD_0963 encodes a 45 aa
204 hypothetical protein. SPD_1711 (132 aa) was described as a single stranded DNA binding
205 protein and may assist in competence (Attaiech et al., 2011) and SPD_1716 is a 63 aa
206 ortholog of cell wall or choline binding protein in other *Streptococcaceae.*

207 We imaged adherent *S. pneumoniae* with fluorescence microscopy during the
208 indicated time points (**Figure 3C**). Since (i) RFP serves as an accurate proxy for cell
209 number and viability(Kjos et al., 2015), (ii) *hlpA* does not change during early infection
210 (p>0.05, FC<2) and (iii) ratio between the GFP and RFP indicates relative expression of the
211 protein of interests (red circle and line, **Figure 3D**), we were able to quantify the proteins of
212 interest. Gene expression values from the dual RNA-Seq data (blue circles and line, **Figure**
213 **3D**) show a degree of correlation with protein level in three out of the four cases –
214 suggesting that pneumococcal transcriptional changes reflects, to some extent, changes in
215 protein level (Vogel and Marcotte, 2012).

216

217 **Pneumococcal ROS induces expression of glutathione-mediated detoxification**
218 **genes in epithelial cells**

219 Along with pneumococcal adherence and multiplication, we aimed to recapitulate the host
220 response in our model. We hypothesized that the epithelial transcriptome adapts in
221 response to bacterial presence, independent of adherence. To identify the responsive

222 genes, we automatically clustered epithelial working libraries exposed to wild type
223 pneumococci. 242 epithelial genes were co-expressed in a similar manner (**Figure 4A**), i.e.,
224 lowly expressed at 30 mpi then sustained upregulation thereafter. Gene ontology (GO)
225 enrichment(Dennis et al., 2003) indicated that 26 of the subset are associated with
226 oxidation and reduction (p=5.7·10^{-4}). Moreover, 9 genes are associated directly with
227 glutathione, an ubiquitous antioxidant: *GCLC* and *GCLM*, in glutathione biosynthesis; *GPX2*
228 and *MGST2* in detoxification; and *GSR*, *IDH1*, *IDH2*, *PGD* and *G6PD* in glutathione
229 recycling.

230 Glutathione, a tripeptide of glutamic acid, cysteine and glycine, is produced and
231 secreted by epithelial cells (Valko et al., 2007). The vital molecule is biosynthesized through
232 amino-acid polymerization and when subjected to ROS (hydrogen peroxide, lipid
233 superoxide or oxygen radicals), glutathione readily donates an electron or hydrogen atom to
234 quench the ROS. The process is assisted by ligands and glutathione peroxidase (GPX2).
235 Oxidized glutathione can be recycled by glutathione reductase (GSR) dependent on
236 NADPH (**Figure 4B**). Alternatively, glutathione conjugates and neutralize ROS(Forman et
237 al., 2009). Expression of nine glutathione-associated genes showed a sustained significant
238 increase in epithelial cells exposed to encapsulated strain (p<0.05, 60 vs. 30 mpi, **Figure**
239 **4C**).

240 To validate the abovementioned finding, we repeated the experiment, isolated total
241 RNA and performed qRT-PCR on four genes: *GPX2*, involved in detoxification and *GSR*,
242 *IDH1* and *PGD*, in glutathione recycling. As expected, we observed significant upregulation
243 of these genes between 30 and 60 mpi (**Figure 4D**). Interestingly, Rai et al showed that
244 pneumococcal supernatant is sufficient to instigate oxidative damage in A549 (Rai et al.,
245 2015). Indeed, when epithelial cells were incubated with filtered pneumococcal

246 supernatants, the genes were activated (**Figure 4D**). To establish that pneumococci-
247 derived ROS was behind the response, we added the antioxidant, resveratrol (100 μM) to
248 the epithelial-pneumococcal model and did not observe activation (**Figure 4D**) (Zahlten et
249 al., 2015).

250

251 **Adherent *S. pneumoniae* repress epithelial innate immune response**

252 Contrasting epithelial gene expression in response to encapsulated and unencapsulated
253 pneumococci allowed us to specifically identify adherence-responsive genes. In doing so,
254 we identified 271 adherence-responsive ($p<0.05$) epithelial genes, of which 25 genes are
255 activated (fold change, $FC>2$) and 248 repressed ($FC>2$) during early-infection (**Figure 5A**).
256 Two genes, *PTGS2* and *HIST1H4B* showed repression and activation at more than one
257 time point. Subsequently, GO-term enrichment in the subset of repressed genes at 60 mpi
258 showed that "immune response" to be enriched in 16 genes ($p=2.3\cdot10^{-4}$, **Figure 5B**).

259 *CXCL8* (*IL8*), encoding interleukin-8, was one of the repressed immunity gene.
260 CXCL8 is a potent chemoattractant for neutrophil and other granulocytes. Interestingly, at
261 60 mpi, Δ*cps2E*-exposed epithelial cells, expressed 2.5±1.3 less *CXCL8* than epithelial
262 cells exposed to wild type *S. pneumoniae* (**Figure 5C**). This difference was validated by
263 qRT-PCR (**Figure 5D**). Further, we asked whether *CXCL8* repression is an active process
264 or merely mediated by physical adherence. To assess this, we co-incubated heat-
265 inactivated Δ*cps2E* and heat-inactivated wild type with epithelial cells. Note that heat
266 inactivation preserves pneumococcal epitope and protein structures (Hvalbye et al., 1999).
267 *CXCL8* was still significantly repressed by dead Δ*cps2E* but not by dead wild type
268 pneumococci (**Figure 5D**) – suggesting that *CXCL8* repression is independent of viability
269 but dependent to presence of the capsule or to the accessibility of surface-exposed

270 (protein) factors in capsule absence. Intriguingly, Graham and Paton showed that epithelial
271 interleukin-8 production and release was suppressed by pneumococcal surface protein
272 CbpA and incubation with Δ*cbpA* leads to higher CXCL8 expression (Graham and Paton,
273 2006). We speculate that the absence of capsule in Δ*cps2E* increases accessibility of
274 pneumococcal surface-exposed factors, including CbpA to epithelial receptors, leading to
275 repression of *CXCL8*.

276 *DEFB1*, encoding β-defensin-1 an important epithelial-derived constitutively-
277 expressed antimicrobial peptide (Krisanaprakornkit et al., 1998), is another repressed
278 immunity gene. However, in our model, *DEFB1* was repressed 3.0±1.2 times ($p<0.05$, 60
279 mpi) in Δ*cps2E*-exposed epithelial cells compared to wild type-exposed cells (**Figure 5C,**
280 validated in **Figure 5D**). Additionally, while heat-inactivated wild type pneumococci
281 stimulate comparable levels of *DEFB1* compared to viable wild type bacteria, non-viable
282 Δ*cps2E* repressed *DEFB1* expression even lower ($p<0.05$) than viable Δ*cps2E* (**Figure**
283 **5D**). We conclude that *DEFB1* expression is affected by adherence, accessibility of
284 pneumococcal surface proteins and pneumococcal viability by an as of yet unknown
285 mechanism. In summary, we show that adherent pneumococci modulate epithelial
286 expression of innate immunity genes, including *CXCL8* and *DEFB1*, mediated by
287 pneumococcal surface factors.

288 **Adherent *S. pneumoniae* activate sugar-importers**

289 Consistent to the epithelial analysis, we contrasted pneumococcal gene expression
290 between unencapsulated and encapsulated libraries, resulting in 248 differentially
291 expressed ($p<0.05$) genes. Specifically, 110 pneumococcal genes of the 248 were
292 activated (*FC*>2) in the unencapsulated strain while 133 genes were repressed (*FC*>2,
293 **Figure 6A**). Five genes, SPD_0188, SPD_0226, SPD_0415, SPD_1717 and SPD_1988,

294 showed repression and activation at different time points. We used gene classes developed
295 for *S. pneumoniae* TIGR4 (van Opijnen and Camilli, 2012) to categorize adherence-
296 responsive genes (**Figure 6B**). Excitingly, most of the adherence-responsive genes are of
297 unknown function (133 of 248 genes, 54%), highlighting our paucity of knowledge in
298 pneumococcal gene function. A large part of the subset (36 genes, 15%) are involved in
299 cellular transport (**Figure 6B**). Since the pneumococcal genome has an exceptionally high
300 number of carbohydrate transporters (Bidossi et al., 2012), it is not surprising that 15 of the
301 genes encode for sugar transporters (**Figure 6C**).

302 At 60 mpi, 11 carbohydrate transporters were differentially expressed ($p<0.05$,
303 $FC>2$) between Δ*cps2E* and encapsulated pneumococci exposed to epithelial cells. In the
304 presence of high glucose ($2g \cdot L^{-1}$), Δ*cps2E* expressed 1.5 fold less *manLM,* encoding
305 glucose transporters, than encapsulated *S. pneumoniae* (**Figure 6D**). Moreover, seven
306 importers were activated in the adherent strain compared to the free-floating encapsulated
307 strain. The seven non-glucose transporter-genes and their substrates are SPD_0089
308 (disaccharides: galactose, mannose, N-acetylmannosamine), *celC* (disaccharides:
309 cellobiose, gentiobiose), SPD_0232/33/34 (disaccharides: cellobiose), *rafE*
310 (oligosaccharides: raffinose, stachyose, melliobiose) and *malD* (polysaccharides:
311 maltotitriol, maltodextrine, glycogen, **Figure 6D**). At the same time, four genes were
312 repressed in unencapsulated *S. pneumoniae* exposed to human epithelial cells, *glpF*
313 (glycerol) and SPD_0740/41/42 (ribonucleosides). We selected three transporter-genes,
314 *malD* (polysaccharides), *rafE* (oligosaccharides) and SPD_0234 (disaccharides) and
315 validated the abovementioned observations by qRT-PCR (**Figure 6E**).

316 Our data indicate that adherent unencapsulated bacteria detect non-glucose sugars
317 in their immediate vicinity. Epithelial mucus may provide non-glucose carbohydrates

318 (Yesilkaya et al., 2008) and simultaneously limit the interaction of epithelial cells to
319 encapsulated wild type bacteria(Nelson et al., 2007). We, then, removed epithelial-
320 associated mucus by washing the surface with warm PBS and observed that the genes
321 were no longer activated (*FC*<2, **Figure 6E**). Next, we incubated pneumococcal strains with
322 type III porcine mucin (5 $g \cdot L^{-1}$), mimicking complex carbohydrate in the medium.
323 Interestingly, the importers were not differentially expressed between strains (*FC*<2),
324 indicating similar access to non-glucose sugars (**Figure 6E**). We conclude that following
325 adherence, *S. pneumoniae* senses an enriched host-derived non-glucose carbohydrate and
326 in turn, activates transporters to import the now-available sugars.

327

328 ## Discussion

329 Early infection is a chaotic and disruptive encounter between host and pathogen. In both
330 species, a multitude of transcriptional-mediated cellular processes are fine-tuned: activated,
331 maintained and repressed to ensure survival. The recently-described dual RNA-Seq
332 approach allows simultaneous host-pathogen monitoring during their interactions (Baddal et
333 al., 2015; Dillon et al., 2015; Westermann et al., 2016). In this study, we exploited the dual
334 RNA-Seq approach by application to a pneumococcal infection model to human lung
335 alveolar epithelial cells. We have generated a detailed time-resolved dataset of epithelial-
336 pneumococcal transcriptomes up to 4 hours after infection. Moreover, we have validated
337 the rich dataset by qRT-PCR and quantitative fluorescence microscopy. Furthermore, we
338 have shown that adherence-specific transcriptional responses in host and pathogen can be
339 identified by contrasting the transcriptomes of the encapsulated libraries with its
340 unencapsulated counterpart.

341 Our early-infection model recapitulated three major *in vivo* characteristics of
342 pneumococcal infection: pneumococcal adhesion, bacterial multiplication and epithelial
343 responses to pathogenic burden. Our model recapitulated these infection characteristics: (i)
344 adherence for both encapsulated and unencapsulated pneumococci (**Figure 1**), (ii)
345 pneumococcal viability and growth during early infection, e.g.: generation of ROS,
346 expression of carbohydrate importers (**Figures 4** and **6**) and (iii) host response to
347 pneumococcal presence, e.g.: glutathione-associated detoxification and innate immune
348 response (**Figures 4** and **5**). Further, as shown by regulation of carbohydrate transporters
349 (**Figure 6**), pneumococci sensed epithelial presence and subsequently adapted their
350 transcriptome.

351 Remarkably, we observed almost all (99%) pneumococcal genes are expressed at
352 early infection (**Figure 2**) – in line with recent studies on bacterial transcriptomes adapting
353 to multiple conditions(Kröger et al., 2013; Nicolas et al., 2012). We speculate that
354 interspecies interaction necessitates massive pneumococcal transcriptional adaptation.
355 Moreover, we have observed activation of detoxification genes (*GPX2* and *GSR*) in
356 epithelial cells protecting against pneumococci-derived ROS (**Figure 4**). Indeed, *S.*
357 *pneumoniae* has been reported to secrete high levels of peroxides as a by-product of its
358 pyruvate metabolism (Carvalho et al., 2011) and has recently been shown to cause DNA-
359 damage-dependent apoptosis in alveolar lung epithelial cells(Rai et al., 2015). In addition,
360 pneumococcal early competence genes (Martin et al., 2000) were activated in our model
361 (http://dualrnaseq.molgenrug.nl competence subset). Future work should also examine
362 whether small non-coding RNAs play a role in pneumococcal early infection as they do in
363 Salmonella (Westermann et al., 2016), something that was not explored currently due to the
364 poor D39 genome annotation in this regard.

365 Our approach can be expanded further by incorporating relevant LRTI agents into
366 the model. For example, alveolar macrophages and epithelial cells, together, form
367 epithelium lining of the lower respiratory tract. The cells reciprocally influence cellular
368 phenotypes and behaviors (Hussell and Bell, 2014), highly relevant to infection. Moreover,
369 pneumococcal co-infection and secondary infection are not unheard of. Influenzae virus
370 potentiates *S. pneumoniae* by neuraminidase activity that exposes cryptic epithelial
371 receptor and facilitates pneumococcal adherence(Siegel et al., 2014). In addition,
372 influenzae infection causes loss of superficial epithelial cells, revealing basal epithelium
373 (Kash et al., 2011) and aggravating secondary pneumococcal infection. On the other hand,
374 *H. influenzae* negatively affects pneumococci by recruiting neutrophils and stimulating the
375 killing of opsonized pneumococci(Lysenko et al., 2010). Incorporation of other agents into
376 the model and exploiting dual (or triple, quadruple) RNA-Seq approaches may provide
377 novel insights into respiratory infection.

378 However, complementary approaches, are needed to obtain a full picture of early
379 infection. Though transcriptome rewiring is a focal point during interspecies interaction
380 (Jenner and Young, 2005; Sorek and Cossart, 2010), non-transcriptional regulation plays
381 an important part during early infection. Capsule shedding, a hallmark of pneumococcal
382 infection, is regulated by autolysin-A (Lyt-A). LytA is activated when the bacterium
383 encounters alveolar cathelicidin (Kietzman et al., 2016), which is independent of
384 transcriptional regulation. Heterogeneity of cellular responses is another confounding factor
385 (Jørgensen et al., 2013). Recently, dual RNA-Seq combined with cell sorting was used to
386 identify heterogeneous activity of Salmonella virulence factor that, in turn, drives
387 heterogeneous interferons response in macrophage(Avraham et al., 2015). This highlights
388 the relevance of noise in gene expression and cell-to-cell variability in host-pathogen
389 interaction. Furthermore, whole organism infection models offers a more systemic

390 perspective. Dual RNA-Seq approach has been used to monitor infection in wheat-bacteria
391 (Camilios-Neto et al., 2014) and mosquito-filaria (Choi et al., 2014). Whole organism dual
392 RNA-Seq is not without its challenges, including averaging (host) effects to gene
393 expression across all cell types.

394 Besides its relevance in communicable diseases, gained insights into pneumococcal
395 infection are also applicable to understanding several non-communicable respiratory
396 diseases. Asthma, the most common chronic respiratory disease is a major risk factor for
397 pneumococcal infection (Talbot et al., 2005). Additionally, COPD (Chronic Obstructive
398 Pulmonary Disease, Decramer et al., 2012) and cigarette smoking (Phipps et al., 2010)
399 have been reported to increase the risk of pneumococcal LRTI. Here, we reported the first
400 study to show simultaneous transcriptomic changes of the pathogen *S. pneumoniae* and
401 human lung alveolar epithelial cells during early infection. Additionally, we have made the
402 time-resolved dual transcriptomics dataset available to the broader research community
403 (http://dualrnaseq.molgenrug.nl). We invite pneumococcal researchers to use the database
404 to formulate research questions in the development of preventive and curative strategies
405 against pneumococcal infection. To conclude, we call researchers from the fields of
406 microbiology, immunology and pulmonology to access the dataset and use it to develop
407 their own hypotheses.

408

409

410 # Methods

411 **Culture of epithelial cell line, *S. pneumoniae* D39 and pneumococcal transformation**

412 Human type II lung epithelial cell line, A549 (ATCC® CCL-185) and *S. pneumoniae* D39
413 were routinely cultured without antibiotics. Strain construction is described in detail in
414 **Supplemental information**. Oligonucleotides are listed in **Supplemental Table 1** and
415 strains in **Supplemental Table 2**.

416 **Infection studies**

417 Confluent monolayer of A549 was co-incubated with *S. pneumoniae* D39 at multiplicities of
418 infection 10, in 1% fetal bovine serum in RPMI1640 without phenol red. Prior to infection,
419 epithelial monolayer was kept for 10 more days after confluence. To optimize cell-to-cell
420 contact, centrifugation was employed (2000 ×g, 5 min, 4°C). Adherence assays were
421 performed by enumeration of plated cfu in blood agar. More in **Supplemental Information**.

422 **Simultaneous total host-pathogen RNA isolation**

423 Before RNA isolation, samples were treated by saturated ammonium sulfate solution
424 (Korfhage et al., 2002). Cells were disrupted by bead beating, and total RNA was isolated
425 as described in the **Supplemental Information**.

426 **Library preparation, sequencing, data pipeline and online database**

427 Total RNA was dual rRNA-depleted, reverse-transcribed and sequenced on the Illumina
428 NextSeq 500 in 75 nt single end mode. Raw reads were trimmed, aligned into chimeric
429 human-pneumococcus genome. Reads were counted and differential gene expression
430 analysis were performed to epithelial and pneumococcal libraries separately. Automatic
431 clustering and GO enrichment were performed. The online database is built using in-house

432 script. Significantly differentially expressed epithelial and pneumococcal genes are listed in
433 **Supplemental Table 3** and **4**, respectively.

434 **qRT-PCR and quantitative fluorescence microscopy**

435 Infection studies were repeated, total RNA isolated and qRT-PCR is performed. For
436 fluorescence microscopy, infection studies were performed in 8-wells μ-slides (Ibidi, DE).
437 More in **Supplemental Information**.

438

439 Data Access

440 The raw data is accessible at http://www.ncbi.nlm.nih.gov/geo/ with accession number
441 GSE79595.

442 Author Contribution

443 R.A and J.W.V. designed the research, analyzed the data and wrote article. R.A performed
444 research, J.S analyzed the data, S.H. built online database.

445

446 Acknowledgements

447 We thank W.J. Quax and R. Setroikromo (UMCG, Groningen) for the human cell line, V.
448 Benes and B. Haase (GeneCore, EMBL, Heidelberg) for sequencing support, M. Kjos for
449 fruitful discussions and A. de Jong for bioinformatics support. We thank S. El Aidy and L.E.
450 Keller for comments on the manuscript. Work in Veening lab is supported by the EMBO
451 Young Investigator Program, VIDI fellowship (864.12.001) from the Netherlands
452 Organization for Scientific Research, Earth and Life Sciences (NWO-ALW), and ERC
453 Starting Grant 337399-PneumoCell.

454

455 ## Conflict of Interest

456 None

457

458 ## References

459 Abeyta, M., Hardy, G.G., and Yother, J. (2003). Genetic alteration of capsule type but not
460 PspA type affects accessibility of surface-bound complement and surface antigens of
461 *Streptococcus pneumoniae*. Infect. Immun. *71*, 218–225.

462 Attaiech, L., Olivier, A., Mortier-Barrière, I., Soulet, A.-L., Granadel, C., Martin, B., Polard,
463 P., and Claverys, J.-P. (2011). Role of the Single-Stranded DNA–Binding Protein SsbB in
464 Pneumococcal Transformation: Maintenance of a Reservoir for Genetic Plasticity. PLOS
465 Genet *7*, e1002156.

466 Avraham, R., Haseley, N., Brown, D., Penaranda, C., Jijon, H.B., Trombetta, J.J., Satija, R.,
467 Shalek, A.K., Xavier, R.J., Regev, A., et al. (2015). Pathogen Cell-to-Cell Variability Drives
468 Heterogeneity in Host Immune Responses. Cell *162*, 1309–1321.

469 Baddal, B., Muzzi, A., Censini, S., Calogero, R.A., Torricelli, G., Guidotti, S., Taddei, A.R.,
470 Covacci, A., Pizza, M., Rappuoli, R., et al. (2015). Dual RNA-seq of Nontypeable
471 *Haemophilus influenzae* and Host Cell Transcriptomes Reveals Novel Insights into Host-
472 Pathogen Cross Talk. mBio *6*, e01765–15.

473 Beiter, K., Wartha, F., Hurwitz, R., Normark, S., Zychlinsky, A., and Henriques-Normark, B.
474 (2008). The Capsule Sensitizes *Streptococcus pneumoniae* to α-Defensins Human
475 Neutrophil Proteins 1 to 3. Infect. Immun. *76*, 3710–3716.

476 Bidossi, A., Mulas, L., Decorosi, F., Colomba, L., Ricci, S., Pozzi, G., Deutscher, J., Viti, C.,
477 and Oggioni, M.R. (2012). A Functional Genomics Approach to Establish the Complement
478 of Carbohydrate Transporters in *Streptococcus pneumoniae* . PLoS ONE *7*, e33320.

479 Bogaert, D., De Groot, R., and Hermans, P.W.M. (2004). *Streptococcus pneumoniae*
480 colonisation: the key to pneumococcal disease. Lancet Infect. Dis. *4*, 144–154.

481 Bolger, A.M., Lohse, M., and Usadel, B. (2014). Trimmomatic: A flexible trimmer for Illumina
482 Sequence Data. Bioinformatics btu170.

483 Bootsma, H.J., Egmont-Petersen, M., and Hermans, P.W.M. (2007). Analysis of the In Vitro
484 Transcriptional Response of Human Pharyngeal Epithelial Cells to Adherent *Streptococcus*
485 *pneumoniae*: Evidence for a Distinct Response to Encapsulated Strains. Infect. Immun. *75*,
486 5489–5499.

487 Camilios-Neto, D., Bonato, P., Wassem, R., Tadra-Sfeir, M.Z., Brusamarello-Santos, L.C.,
488 Valdameri, G., Donatti, L., Faoro, H., Weiss, V.A., Chubatsu, L.S., et al. (2014). Dual RNA-

489 seq transcriptional analysis of wheat roots colonized by *Azospirillum brasilense* reveals up-
490 regulation of nutrient acquisition and cell cycle genes. BMC Genomics *15*, 378.

491 Carvalho, S.M., Kloosterman, T.G., Kuipers, O.P., and Neves, A.R. (2011). CcpA Ensures
492 Optimal Metabolic Fitness of *Streptococcus pneumoniae*. PLoS ONE *6*, e26707.

493 Choi, Y.-J., Aliota, M.T., Mayhew, G.F., Erickson, S.M., and Christensen, B.M. (2014). Dual
494 RNA-seq of Parasite and Host Reveals Gene Expression Dynamics during Filarial Worm–
495 Mosquito Interactions. PLOS Negl Trop Dis *8*, e2905.

496 Decramer, M., Janssens, W., and Miravitlles, M. (2012). Chronic obstructive pulmonary
497 disease. The Lancet *379*, 1341–1351.

498 Dennis, G., Sherman, B.T., Hosack, D.A., Yang, J., Gao, W., Lane, H.C., and Lempicki,
499 R.A. (2003). DAVID: Database for Annotation, Visualization, and Integrated Discovery.
500 Genome Biol. *4*, P3.

501 Dillon, L.A.L., Suresh, R., Okrah, K., Corrada Bravo, H., Mosser, D.M., and El-Sayed, N.M.
502 (2015). Simultaneous transcriptional profiling of *Leishmania major* and its murine
503 macrophage host cell reveals insights into host-pathogen interactions. BMC Genomics *16*,
504 1108.

505 Dobin, A., Davis, C.A., Schlesinger, F., Drenkow, J., Zaleski, C., Jha, S., Batut, P.,
506 Chaisson, M., and Gingeras, T.R. (2013). STAR: ultrafast universal RNA-seq aligner.
507 Bioinforma. Oxf. Engl. *29*, 15–21.

508 Forman, H.J., Zhang, H., and Rinna, A. (2009). Glutathione: Overview of its protective
509 roles, measurement, and biosynthesis. Mol. Aspects Med. *30*, 1–12.

510 Graham, R.M.A., and Paton, J.C. (2006). Differential Role of CbpA and PspA in Modulation
511 of In Vitro CXC Chemokine Responses of Respiratory Epithelial Cells to Infection with
512 *Streptococcus pneumoniae*. Infect. Immun. *74*, 6739–6749.

513 Gray, R.D., Duncan, A., Noble, D., Imrie, M., O'Reilly, D.S.J., Innes, J.A., Porteous, D.J.,
514 Greening, A.P., and Boyd, A.C. (2010). Sputum trace metals are biomarkers of
515 inflammatory and suppurative lung disease. Chest *137*, 635–641.

516 Hackett, N.R., Butler, M.W., Shaykhiev, R., Salit, J., Omberg, L., Rodriguez-Flores, J.L.,
517 Mezey, J.G., Strulovici-Barel, Y., Wang, G., Didon, L., et al. (2012). RNA-Seq quantification
518 of the human small airway epithelium transcriptome. BMC Genomics *13*, 82.

519 Hallstrand, T.S., Hackett, T.L., Altemeier, W.A., Matute-Bello, G., Hansbro, P.M., and
520 Knight, D.A. (2014). Airway epithelial regulation of pulmonary immune homeostasis and
521 inflammation. Clin. Immunol. Orlando Fla *151*, 1–15.

522 Hammerschmidt, S., Bergmann, S., Paterson, G.K., and Mitchell, T.J. (2007). Pathogenesis
523 of *Streptococcus pneumoniae* infections :adaptive immunity, innate immunity, cell biology,
524 virulence factors. In Community-Acquired Pneumonia, (Birkhäuser Basel), pp. 139–181.

525 Hussell, T., and Bell, T.J. (2014). Alveolar macrophages: plasticity in a tissue-specific
526 context. Nat. Rev. Immunol. *14*, 81–93.

527 Hvalbye, B.K.R., Aaberge, I.S., Løvik, M., and Haneberg, B. (1999). Intranasal
528 Immunization with Heat-Inactivated *Streptococcus pneumoniae* Protects Mice against
529 Systemic Pneumococcal Infection. Infect. Immun. *67*, 4320–4325.

530 Hyams, C., Camberlein, E., Cohen, J.M., Bax, K., and Brown, J.S. (2010). The
531 *Streptococcus pneumoniae* Capsule Inhibits Complement Activity and Neutrophil
532 Phagocytosis by Multiple Mechanisms. Infect. Immun. *78*, 704–715.

533 Jenner, R.G., and Young, R.A. (2005). Insights into host responses against pathogens from
534 transcriptional profiling. Nat. Rev. Microbiol. *3*, 281–294.

535 Jørgensen, M.G., van Raaphorst, R., and Veening, J.-W. (2013). Chapter 6 - Noise and
536 Stochasticity in Gene Expression: A Pathogenic Fate Determinant. In Methods in
537 Microbiology, C.H. and A. Wipat, ed. (Academic Press), pp. 157–175.

538 Kadioglu, A., Weiser, J.N., Paton, J.C., and Andrew, P.W. (2008). The role of
539 *Streptococcus pneumoniae* virulence factors in host respiratory colonization and disease.
540 Nat. Rev. Microbiol. *6*, 288–301.

541 Kash, J.C., Walters, K.-A., Davis, A.S., Sandouk, A., Schwartzman, L.M., Jagger, B.W.,
542 Chertow, D.S., Li, Q., Kuestner, R.E., Ozinsky, A., et al. (2011). Lethal synergism of 2009
543 pandemic H1N1 influenza virus and *Streptococcus pneumoniae* coinfection is associated
544 with loss of murine lung repair responses. mBio *2*.

545 Kietzman, C.C., Gao, G., Mann, B., Myers, L., and Tuomanen, E.I. (2016). Dynamic
546 capsule restructuring by the main pneumococcal autolysin LytA in response to the
547 epithelium. Nat. Commun. *7*, 10859.

548 Kjos, M., Aprianto, R., Fernandes, V.E., Andrew, P.W., van Strijp, J.A.G., Nijland, R., and
549 Veening, J.-W. (2015). Bright fluorescent *Streptococcus pneumoniae* for live-cell imaging of
550 host-pathogen interactions. J. Bacteriol. *197*, 807–818.

551 Korfhage, C., Wyrich, R., and Oelmuller, U. (2002). Ammonium sulfate for neutralization of
552 inhibitory effects (Google Patents).

553 Krisanaprakornkit, S., Weinberg, A., Perez, C.N., and Dale, B.A. (1998). Expression of the
554 peptide antibiotic human beta-defensin 1 in cultured gingival epithelial cells and gingival
555 tissue. Infect. Immun. *66*, 4222–4228.

556 Kröger, C., Colgan, A., Srikumar, S., Händler, K., Sivasankaran, S.K., Hammarlöf, D.L.,
557 Canals, R., Grissom, J.E., Conway, T., Hokamp, K., et al. (2013). An Infection-Relevant
558 Transcriptomic Compendium for *Salmonella enterica* Serovar Typhimurium. Cell Host
559 Microbe *14*, 683–695.

560 Kukurba, K.R., and Montgomery, S.B. (2015). RNA Sequencing and Analysis. Cold Spring
561 Harb. Protoc. *2015*, pdb.top084970.

562 Kumar, L., and E. Futschik, M. (2007). Mfuzz: A software package for soft clustering of
563 microarray data. Bioinformation *2*, 5–7.

564 Lee, H.-Y., Andalibi, A., Webster, P., Moon, S.-K., Teufert, K., Kang, S.-H., Li, J.-D.,
565 Nagura, M., Ganz, T., and Lim, D.J. (2004). Antimicrobial activity of innate immune

566 molecules against *Streptococcus pneumoniae, Moraxella catarrhalis* and nontypeable
567 *Haemophilus influenzae*. BMC Infect. Dis. *4*, 12.

568 Liao, Y., Smyth, G.K., and Shi, W. (2014). featureCounts: an efficient general purpose
569 program for assigning sequence reads to genomic features. Bioinforma. Oxf. Engl. *30*, 923–
570 930.

571 Livak, K.J., and Schmittgen, T.D. (2001). Analysis of relative gene expression data using
572 real-time quantitative PCR and the 2(-Delta Delta C(T)) Method. Methods San Diego Calif
573 *25*, 402–408.

574 Love, M.I., Huber, W., and Anders, S. (2014). Moderated estimation of fold change and
575 dispersion for RNA-seq data with DESeq2. Genome Biol. *15*, 550.

576 Lysenko, E.S., Lijek, R.S., Brown, S.P., and Weiser, J.N. (2010). Within-Host Competition
577 Drives Selection for the Capsule Virulence Determinant of *Streptococcus pneumoniae*.
578 Curr. Biol. *20*, 1222–1226.

579 Martin, B., Prudhomme, M., Alloing, G., Granadel, C., and Claverys, J.P. (2000). Cross-
580 regulation of competence pheromone production and export in the early control of
581 transformation in *Streptococcus pneumoniae*. Mol. Microbiol. *38*, 867–878.

582 Mlacha, S.Z.K., Romero-Steiner, S., Hotopp, J.C.D., Kumar, N., Ishmael, N., Riley, D.R.,
583 Farooq, U., Creasy, T.H., Tallon, L.J., and Liu, X. (2013). Phenotypic, genomic, and
584 transcriptional characterization of *Streptococcus pneumoniae* interacting with human
585 pharyngeal cells. BMC Genomics *14*, 383.

586 Nelson, A.L., Roche, A.M., Gould, J.M., Chim, K., Ratner, A.J., and Weiser, J.N. (2007).
587 Capsule enhances pneumococcal colonization by limiting mucus-mediated clearance.
588 Infect. Immun. *75*, 83–90.

589 Nicolas, P., Mäder, U., Dervyn, E., Rochat, T., Leduc, A., Pigeonneau, N., Bidnenko, E.,
590 Marchadier, E., Hoebeke, M., Aymerich, S., et al. (2012). Condition-dependent
591 transcriptome reveals high-level regulatory architecture in *Bacillus subtilis*. Science *335*,
592 1103–1106.

593 Ning, K., Fermin, D., and Nesvizhskii, A.I. (2012). Comparative analysis of different label-
594 free mass spectrometry based protein abundance estimates and their correlation with RNA-
595 Seq gene expression data. J. Proteome Res. *11*, 2261–2271.

596 van Opijnen, T., and Camilli, A. (2012). A fine scale phenotype-genotype virulence map of a
597 bacterial pathogen. Genome Res. *22*, 2541–2551.

598 Pedersen, M., Nissen, S., Mitarai, N., Svenningsen, S.L., Sneppen, K., and Pedersen, S.
599 (2011). The Functional Half-Life of an mRNA Depends on the Ribosome Spacing in an
600 Early Coding Region. J. Mol. Biol. *407*, 35–44.

601 Phipps, J.C., Aronoff, D.M., Curtis, J.L., Goel, D., O'Brien, E., and Mancuso, P. (2010).
602 Cigarette Smoke Exposure Impairs Pulmonary Bacterial Clearance and Alveolar
603 Macrophage Complement-Mediated Phagocytosis of *Streptococcus pneumoniae*. Infect.
604 Immun. *78*, 1214–1220.

605 Prina, E., Ranzani, O.T., and Torres, A. (2015). Community-acquired pneumonia. The
606 Lancet *386*, 1097–1108.

607 Rai, P., Parrish, M., Tay, I.J.J., Li, N., Ackerman, S., He, F., Kwang, J., Chow, V.T., and
608 Engelward, B.P. (2015). *Streptococcus pneumoniae* secretes hydrogen peroxide leading to
609 DNA damage and apoptosis in lung cells. Proc. Natl. Acad. Sci. *112*, E3421–E3430.

610 Rajam, G., Anderton, J.M., Carlone, G.M., Sampson, J.S., and Ades, E.W. (2008).
611 Pneumococcal surface adhesin A (PsaA): a review. Crit. Rev. Microbiol. *34*, 131–142.

612 Rose, M.C., and Voynow, J.A. (2006). Respiratory tract mucin genes and mucin
613 glycoproteins in health and disease. Physiol. Rev. *86*, 245–278.

614 Shelburne, S.A., Davenport, M.T., Keith, D.B., and Musser, J.M. (2008). The role of
615 complex carbohydrate catabolism in the pathogenesis of invasive streptococci. Trends
616 Microbiol. *16*, 318–325.

617 Siegel, S.J., Roche, A.M., and Weiser, J.N. (2014). Influenza promotes pneumococcal
618 growth during coinfection by providing host sialylated substrates as a nutrient source. Cell
619 Host Microbe *16*, 55–67.

620 Sorek, R., and Cossart, P. (2010). Prokaryotic transcriptomics: a new view on regulation,
621 physiology and pathogenicity. Nat. Rev. Genet. *11*, 9–16.

622 Soumelis, V., Reche, P.A., Kanzler, H., Yuan, W., Edward, G., Homey, B., Gilliet, M., Ho,
623 S., Antonenko, S., Lauerma, A., et al. (2002). Human epithelial cells trigger dendritic cell
624 mediated allergic inflammation by producing TSLP. Nat. Immunol. *3*, 673–680.

625 St-Pierre, C., Brochu, S., Vanegas, J.R., Dumont-Lagacé, M., Lemieux, S., and Perreault,
626 C. (2013). Transcriptome sequencing of neonatal thymic epithelial cells. Sci. Rep. *3*, 1860.

627 Talbot, T.R., Hartert, T.V., Mitchel, E., Halasa, N.B., Arbogast, P.G., Poehling, K.A.,
628 Schaffner, W., Craig, A.S., and Griffin, M.R. (2005). Asthma as a risk factor for invasive
629 pneumococcal disease. N. Engl. J. Med. *352*, 2082–2090.

630 Taniguchi, Y., Choi, P.J., Li, G.-W., Chen, H., Babu, M., Hearn, J., Emili, A., and Xie, X.S.
631 (2010). Quantifying *E. coli* proteome and transcriptome with single-molecule sensitivity in
632 single cells. Science *329*, 533–538.

633 Tecle, T., Tripathi, S., and Hartshorn, K.L. (2010). Review: Defensins and cathelicidins in
634 lung immunity. Innate Immun. *16*, 151–159.

635 The ENCODE Consortium (2011). Standards, Guidelines and Best Practices for RNA-Seq.

636 Tseng, H.-J., McEwan, A.G., Paton, J.C., and Jennings, M.P. (2002). Virulence of
637 *Streptococcus pneumoniae*: PsaA mutants are hypersensitive to oxidative stress. Infect.
638 Immun. *70*, 1635–1639.

639 Valko, M., Leibfritz, D., Moncol, J., Cronin, M.T.D., Mazur, M., and Telser, J. (2007). Free
640 radicals and antioxidants in normal physiological functions and human disease. Int. J.
641 Biochem. Cell Biol. *39*, 44–84.

642 Vogel, C., and Marcotte, E.M. (2012). Insights into the regulation of protein abundance from
643 proteomic and transcriptomic analyses. Nat. Rev. Genet. *13*, 227–232.

644 Voynow, J.A., and Rubin, B.K. (2009). Mucins, Mucus, and Sputum. Chest *135*, 505–512.

645 Wagner, G.P., Kin, K., and Lynch, V.J. (2012). Measurement of mRNA abundance using
646 RNA-seq data: RPKM measure is inconsistent among samples. Theory Biosci. Theor. Den
647 Biowissenschaften *131*, 281–285.

648 Westermann, A.J., Gorski, S.A., and Vogel, J. (2012). Dual RNA-seq of pathogen and host.
649 Nat. Rev. Microbiol. *10*, 618–630.

650 Westermann, A.J., Förstner, K.U., Amman, F., Barquist, L., Chao, Y., Schulte, L.N., Müller,
651 L., Reinhardt, R., Stadler, P.F., and Vogel, J. (2016). Dual RNA-seq unveils noncoding RNA
652 functions in host-pathogen interactions. Nature *529*, 496–501.

653 Yesilkaya, H., Manco, S., Kadioglu, A., Terra, V.S., and Andrew, P.W. (2008). The ability to
654 utilize mucin affects the regulation of virulence gene expression in *Streptococcus*
655 *pneumoniae*. FEMS Microbiol. Lett. *278*, 231–235.

656 Zahlten, J., Kim, Y.-J., Doehn, J.-M., Pribyl, T., Hocke, A.C., García, P., Hammerschmidt,
657 S., Suttorp, N., Hippenstiel, S., and Hübner, R.-H. (2015). *Streptococcus pneumoniae*-
658 Induced Oxidative Stress in Lung Epithelial Cells Depends on Pneumococcal Autolysis and
659 Is Reversible by Resveratrol. J. Infect. Dis. *211*, 1822–1830.

660

661 ## Figures and Legends

662

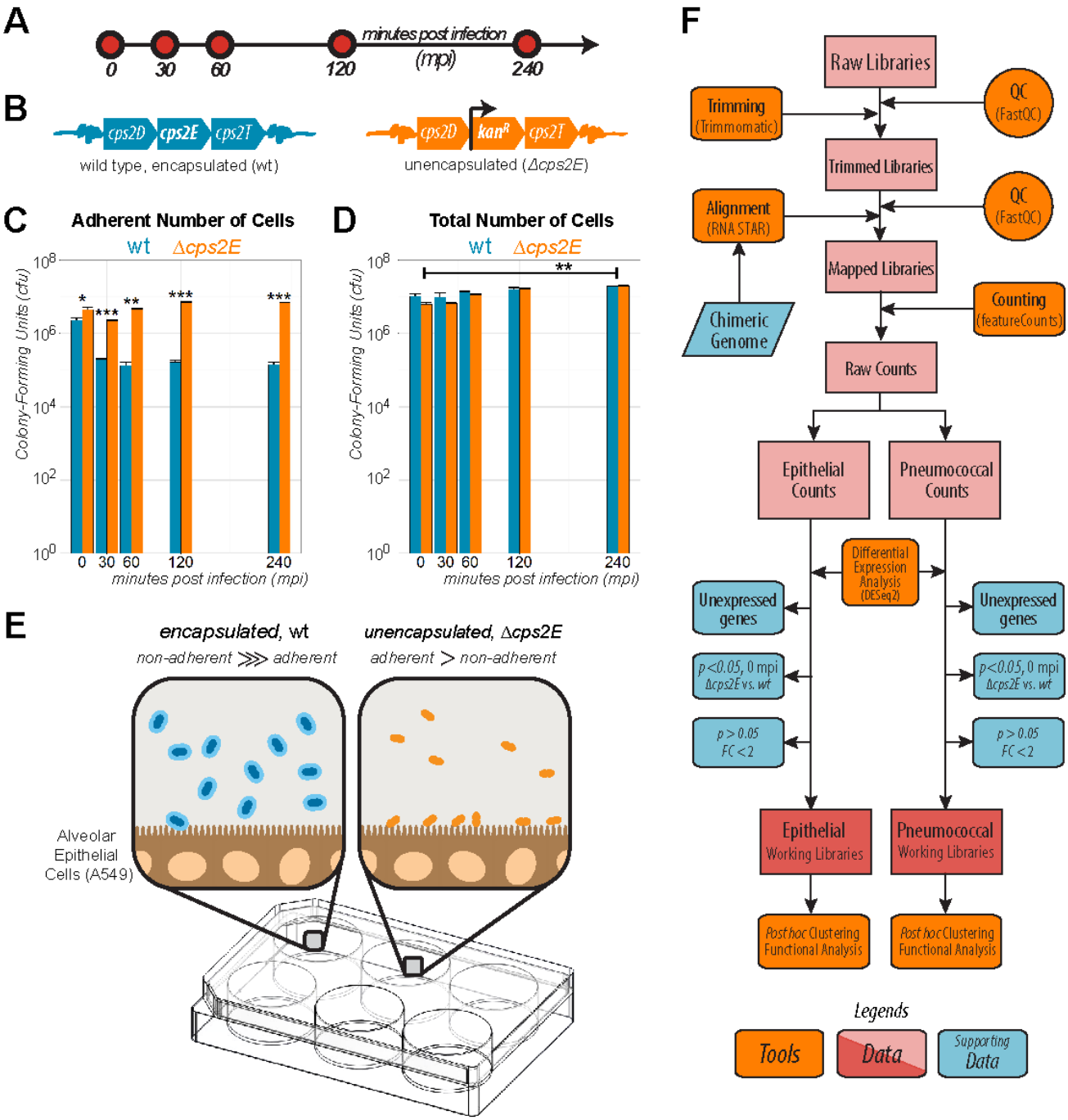

Figure 1. The early infection model. Confluent monolayer of alveolar epithelial cell line (A549) was co-incubated with *S. pneumoniae* strain D39. **A**. We chose five infection time points: 0, 30, 60, 120 and 240 minutes post infection (mpi). **B**. Since adherence is a hallmark of infection, we used an unencapsulated strain, created by disrupting *cps2E* vital

in capsule biogenesis. **C**. Δ*cps2E* strain adhered more readily to epithelial cells than its encapsulated parental strain. 30 mpi, Δ*cps2E* (orange bar) showed significantly ($p<0.001$) more adherent cells than its parental strain (cyan bar). Data is presented as mean±SEM. **D**. At 240 mpi, both strains multiplied significantly ($p<0.01$) with no significant difference between strains. **E**. Encapsulated strain has more free-floating than adherent cells while Δ*cps2E* has a higher fraction of adherent bacteria. **F**. After quality-check, low-quality reads were trimmed. Reads were aligned to a synthetic chimeric genome. Aligned reads were counted and classified as epithelial or as pneumococcal counts. We removed three gene fractions, clustered and performed functional enrichment to the working libraries.

663

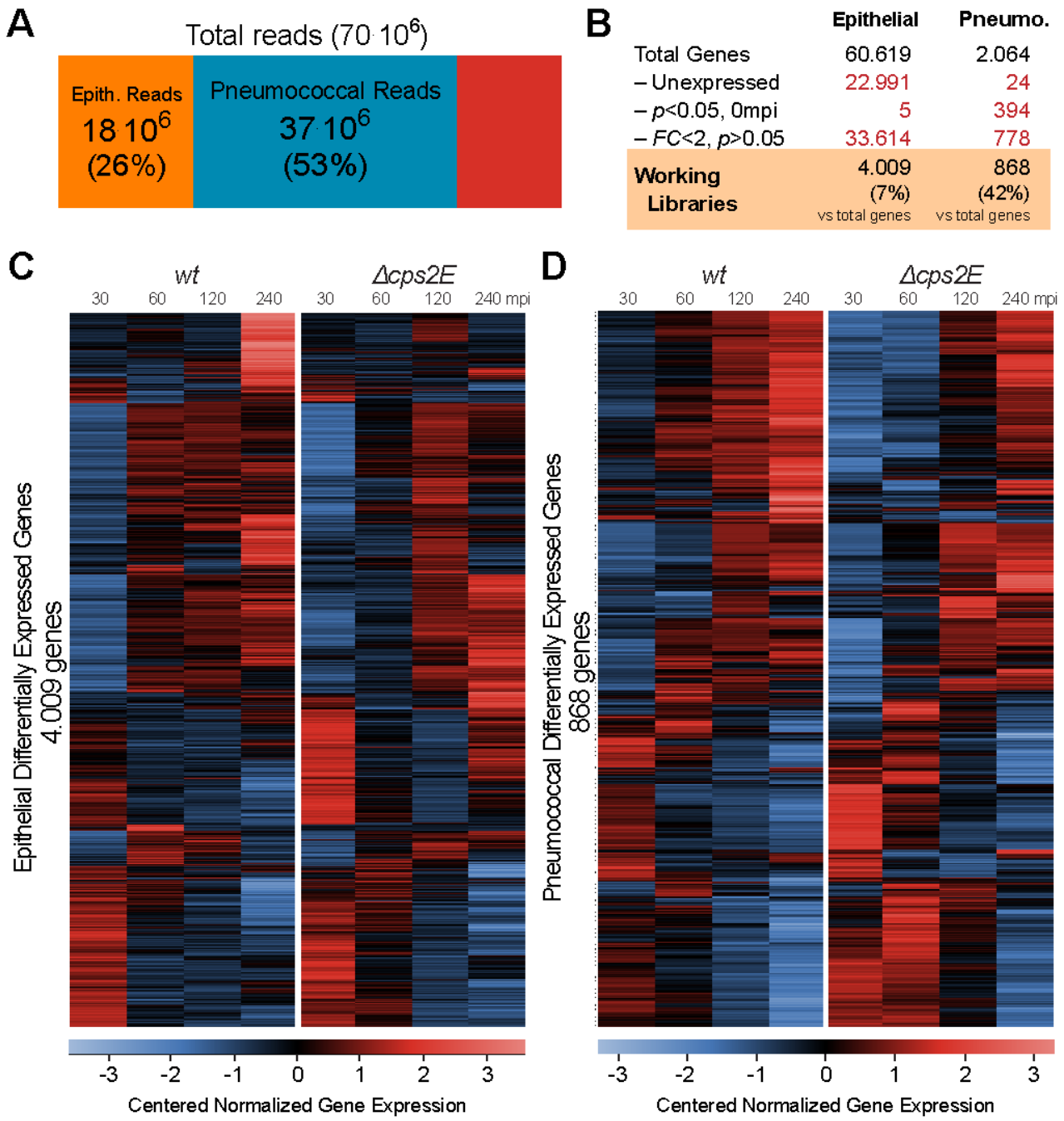

Figure 2. Dual RNA-Seq generates high-quality datasets suitable for probing host-pathogen transcriptomes. A. On average, there are 70 million reads per library: 18 million reads were mapped to the human genome while 37 million reads to pneumococcal genome. **B.** We excluded three gene fractions: unexpressed genes, i.e.: without counts in any libraries; genes that were differentially expressed at 0 mpi (p<0.05) between Δ*cps2E*

and wt libraries and genes with no statistical significance (p>0.05) and fold change less than two (FC<2) in all contrast. Epithelial working libraries contain 4.009 genes (7% of human genes) while pneumococcal working libraries 868 genes (42% pneumococcal genes). **C.** Gene expression in epithelial working libraries were normalized, centered and automatically clustered. The left panel shows epithelial genes in response to encapsulated strain while the right panel shows epithelial response to Δ*cps2E S. pneumoniae* at different time points. Clear clusters of co-expressed epithelial genes can be observed in the heat map. Blue indicates a relatively lower expression while red, a higher value. **D**. Correspondingly, we presented pneumococcal expression in the same manner: left panel shows wild type pneumococcal response to epithelial cells, while right panel shows Δ*cps2E* response.

664

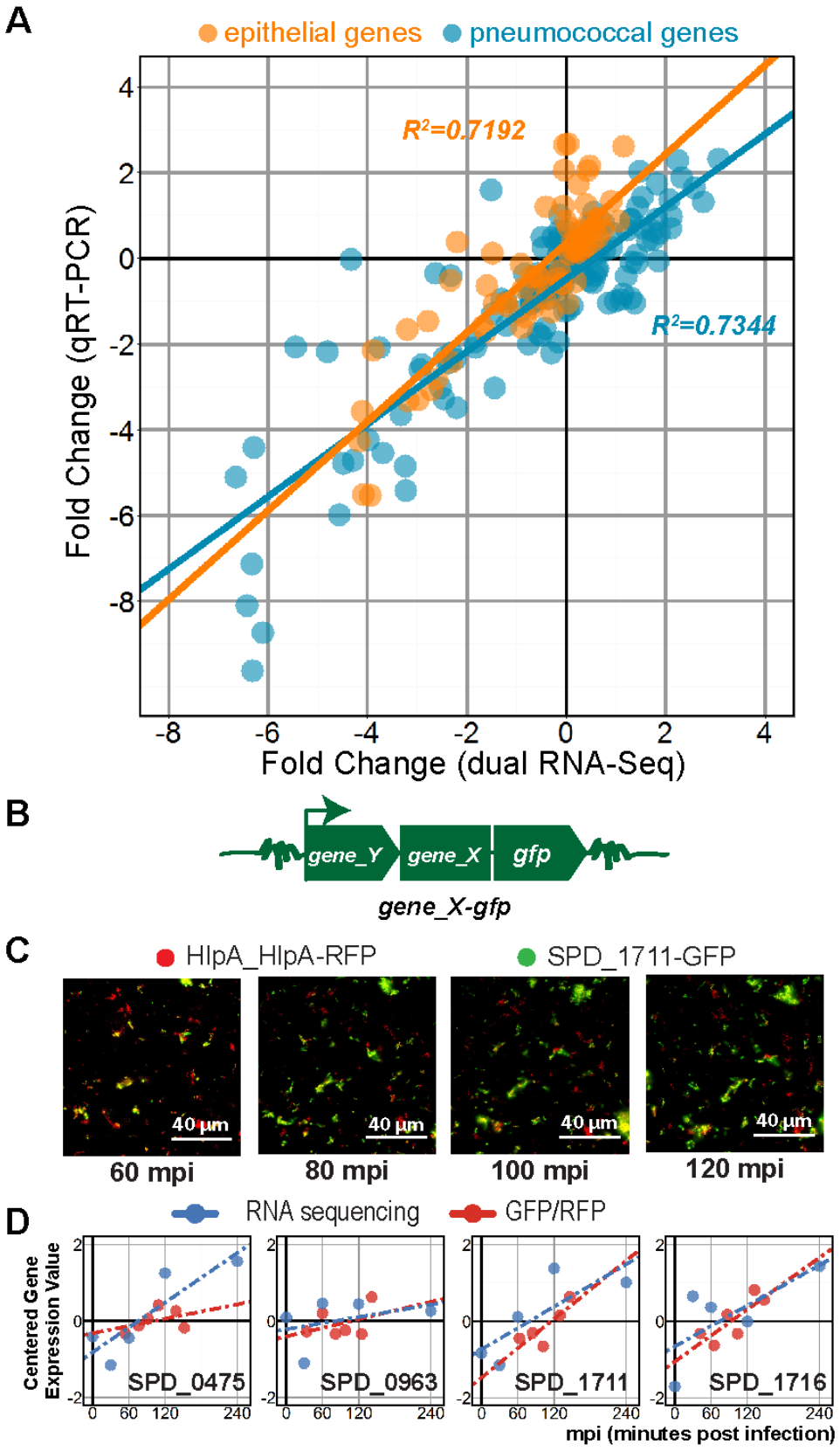

Figure 3. Validation of dual RNA-Seq. A. We confirmed dual RNA-Seq gene expression

values by qRT-PCR. The infection study was repeated in duplicates and total RNA was isolated as previously. Ten human and 19 pneumococcal genes were chosen as validation targets. We plotted fold changes from qRT-PCR against dual RNA-Seq fold changes and observed a high degree of correlation ($R^2 > 0.7$, Pearson) for both species. **B.** We also confirmed pneumococcal gene expression at the protein level by quantitative fluorescence microscopy. Four target genes (SPD_0475, SPD_0963, SPD_1711 and SPD_1716) were C-terminally tagged with GFP at their own locus. GFP-fusion were performed in the Δ*cps2E* strain expressing RFP fused to HlpA. **C.** Non-deconvolved image of SPD_1711-GFP in Δ*cps2E* strain up to 120 mpi. While RFP emitted a relatively constant signal, the GFP signal increases. **D**. We plotted dual RNA-Seq expression values superimposed to the GFP/RFP ratio. To some extent, transcriptional changes corresponded to protein expression.

665

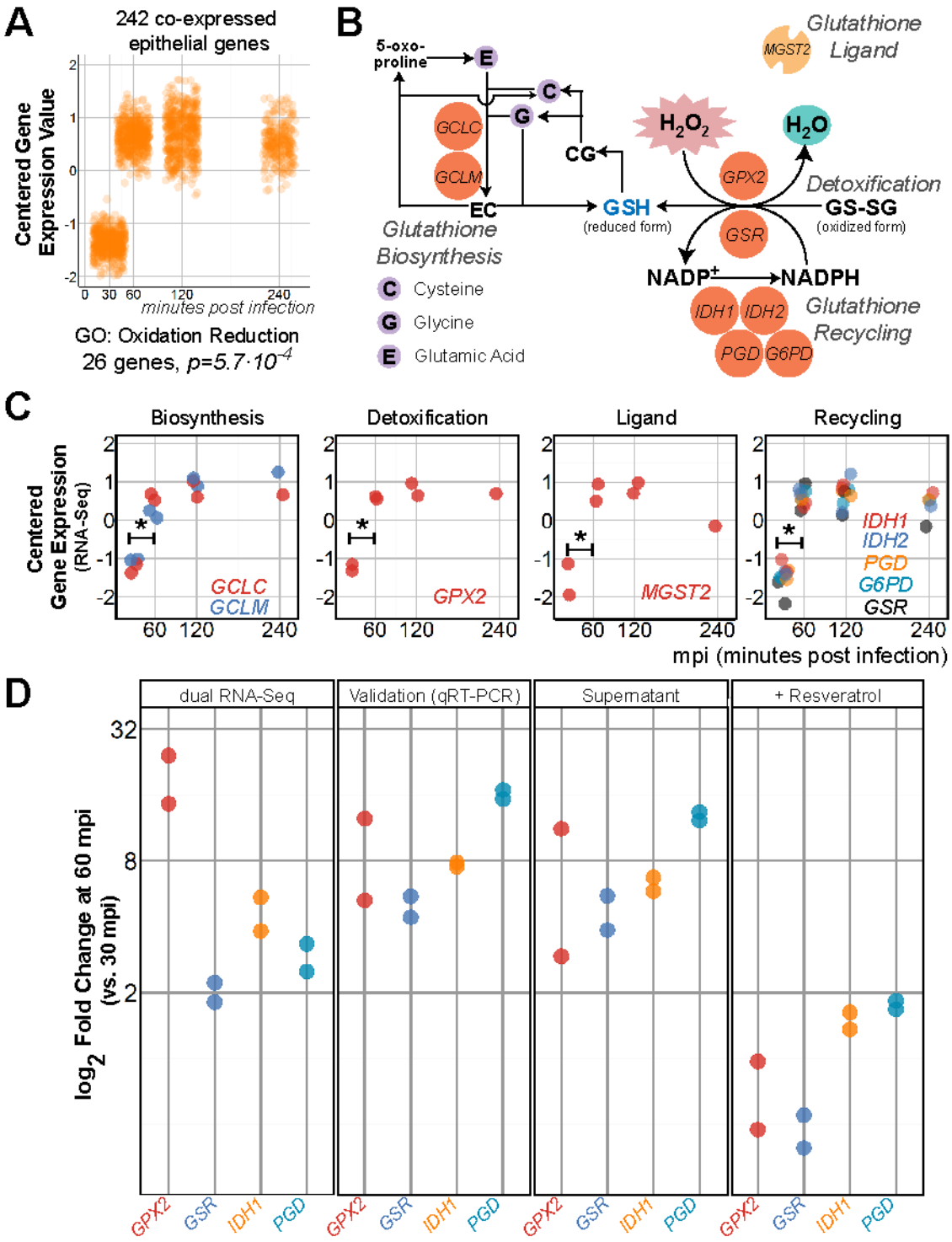

Figure 4. Epithelial glutathione-associated genes are activated in response to pneumococcal ROS. A. We clustered epithelial working libraries exposed to wild type pneumococci and found a cluster of 242 co-expressed genes showing sustained upregulation (p<0.05, FC>2) at 60 mpi compared to 30 mpi. GO analysis showed that

“oxidation reduction” was enriched in 26 genes (p=5.7·10^{-4}). **B**. Nine genes from the subset are associated with glutathione (GSH), an important antioxidant. Main glutathione-associated processes are biosynthesis of glutathione, detoxification of ROS assisted by ligand and glutathione recycling. **C**. Between 30 and 60 mpi, *GCLC* was increased 2.3±1.1 times and *GCLM* 2.4±1.2 times. *GPX2*, the main detoxification gene was activated 18.7±1.3 times while the ligand, *MGST2* 3.2±1.2 times. Genes involved in the recycling of glutathione were activated: *IDH1,* 4.6±1.2; *IDH2*, 2.4±1.2; *PGD,* 2.9±1.2; *G6PD,* 6.6±1.2 and *GSR,* 2.0±1.1 times. **D**. We validated *GPX2*, *GSR, IDH1* and *PGD* expression with qRT-PCR. Epithelial incubation with pneumococcal supernatant showed similar upregulation of glutathione-associated genes. Addition of resveratrol (100μM) into the model diminished the upregulation (FC<2) altogether.

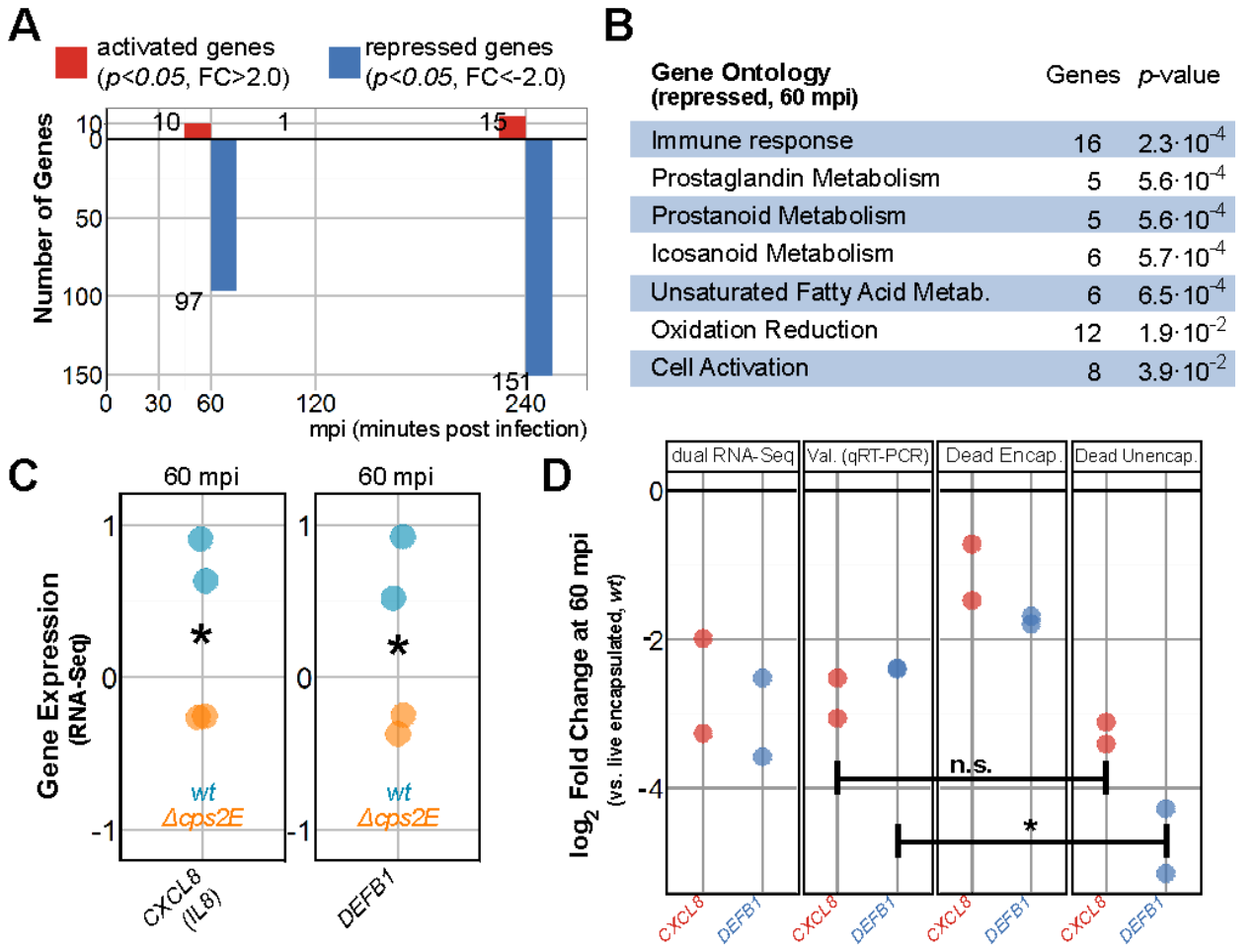

Figure 5. Adherent *S. pneumoniae* repress epithelial innate immune responses. A. At 60 mpi, 97 epithelial genes were significantly repressed upon exposure to Δ*cps2E* bacteria compared to exposure to wild type pneumococci. **B.** GO term enrichment to 60 mpi repressed genes resulted in "immune response" (16 genes, p=2.3·10^{-4}), prostaglandin metabolism (5 genes, p=5.6·10^{-4}) and oxidation reduction (12 genes, p=0.019) among others. **C.** Δ*cps2E*–exposed epithelial cells expressed 2.6±1.3 fold less *CXCL8* and 3.0±1.2 fold less *DEFB1* than wild type-exposed epithelial cells. **D.** We validated *CXCL8* and *DEFB1* repression by qRT-PCR. Heat-inactivated encapsulated bacteria showed no repression of *CXCL8* and *DEFB1,* i.e., no difference (p>0.05) compared to viable encapsulated *S. pneumoniae* (Dead Encap.). While infection with heat-inactivated Δ*cps2E* repressed *CXCL8* to the level of viable Δ*cps2E*, *DEFB1* was more repressed (p<0.05) by

dead Δ*cps2E* than by viable unencapsulated pneumococci.

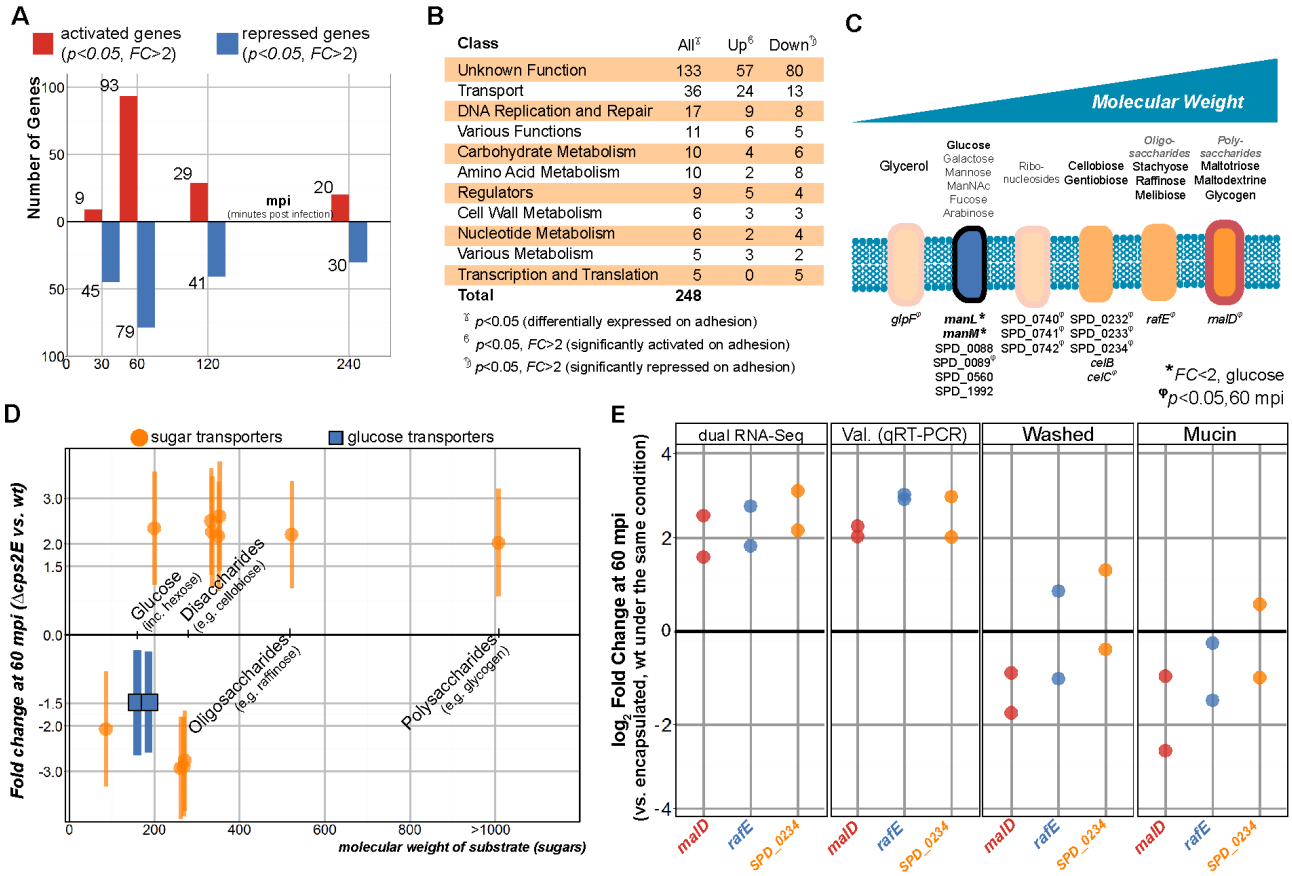

Figure 6. Adherent pneumococci gain access to host-derived carbohydrates and activate non-glucose sugar importers. A. 248 genes were differentially expressed between pneumococcal strains exposed to epithelial cells: 115 genes of the 248 genes were activated in Δ*cps2E* compared to wt pneumococci while 138 genes were repressed. Note that five genes showed activation and repression at different time points. **B.** Most of the differentially-expressed genes are of unknown function (133 genes, 54% of 248), followed by cellular transport (36 genes, 15%) and DNA replication, repair and recombination (17 genes, 7%). **C.** 15 of the 36 transporter genes are described to transport carbohydrate. The carbohydrate-importers transport a wide range of carbohydrates, from

simple monosaccharides to complex polysaccharides. **D.** At 60 mpi, the expression of glucose transporters (*manLM*, blue boxes) is repressed ($p<0.05$, $FC=1.5$) in Δ*cps2E* compared to encapsulated *S. pneumoniae*. Seven non-glucose transporters are activated ($p<0.05$, $FC>2$) in the Δ*cps2E* strain: SPD_0089, *celC,* SPD_0232/33/34*, rafE* and *malD*. **E.** We validated the data by qRT- PCR for three sugar importers: *malD* (polysaccharides)*, rafE* (oligosaccharide), and SPD_0234 (non-glucose disaccharide). By removing epithelial mucus prior to infection, the importers were no longer activated in Δ*cps2E* compared to wild type ($FC<2$, Washed). Incubation with type III porcine mucin ($5 g \cdot L^{-1}$) did not activate the genes in Δ*cps2E* compared to encapsulated pneumococci ($FC<2$).

667